



# Remarkable Removal of Pb(II) Ions from Aqueous Media Using Facilely Synthesized Sodium Manganese Silicate Hydroxide Hydrate/ Manganese Silicate as a Novel Nanocomposite

Ehab A. Abdelrahman<sup>1,2</sup> · Faisal K. Algethami<sup>1</sup> · Huda S. AlSalem<sup>3</sup> · Soha T. Al-Goul<sup>4</sup> · Fawaz A. Saad<sup>5</sup> · Gharieb S. El-Sayyad<sup>6,7</sup> · Reem M. Alghanmi<sup>8</sup> · Khalil ur Rehman<sup>9</sup>

Received: 5 July 2023 / Accepted: 4 October 2023 / Published online: 12 October 2023  
© The Author(s), under exclusive licence to Springer Science+Business Media, LLC, part of Springer Nature 2023

## Abstract

The presence of Pb(II) ions in water causes many diseases, such as anemia, kidney disorders, and nervous system disorders. Therefore, this paper presents the facile hydrothermal synthesis of a novel type of nanocomposites, specifically sodium manganese silicate hydroxide hydrate/manganese silicate nanocomposite ( $\text{Na}_4\text{Mn}_5\text{Si}_{10}\text{O}_{24}(\text{OH})_6 \cdot 6\text{H}_2\text{O}/\text{Mn}^{2+}\text{Mn}_6^{3+}\text{SiO}_{12}$ ), which exhibits remarkable efficiency in the uptake of Pb(II) ions from aqueous solutions. The nanocomposites were chemically constructed using the hydrothermal technique in the absence and presence of polyethylene glycol 400 as an organic template to control the morphology, BET surface area, and mean crystallite size. The nanocomposites, which were chemically fabricated in the absence and presence of polyethylene glycol 400, are abbreviated as NF and NP, respectively. In addition, the XRD analysis exhibited that the calculated mean crystallite size of the NF and NP nanocomposites was found to be 18.28 and 60.26 nm, respectively. Due to the inverse relationship between crystallite size and BET surface area, the NF nanocomposite exhibits a higher BET surface area ( $71.52 \text{ m}^2/\text{g}$ ) compared to the NP nanocomposite ( $46.26 \text{ m}^2/\text{g}$ ). Hence, the greatest uptake capacity of the NF nanocomposite towards Pb(II) ions ( $292.39 \text{ mg/g}$ ) is greater than that of the NP nanocomposite ( $210.97 \text{ mg/g}$ ). Both NF and NP nanocomposites chemically and exothermically capture Pb(II) ions. Also, the adsorption processes obey the pseudo-second-order kinetic model and Langmuir equilibrium isotherm.

**Keywords** Novel adsorbents · Pb(II) ions · Sodium manganese silicate hydroxide hydrate · Manganese silicate

## 1 Introduction

Freshwater scarcity is one of the greatest challenges in the agriculture and food security disciplines. Approximately 300 million North Africans, out of a total population of 800 million, live in areas with limited access to water

resources. Through a vast multitude of industrial activities, heavy metal ions, such as Pb(II), Zn(II), and Cd(II) are released into aquatic ecosystems, where they accumulate in aquatic habitats [1]. Due to their toxicity, heavy metals pose a problem for ecosystems, and the vast majority of heavy metals are extremely poisonous even at very

✉ Ehab A. Abdelrahman  
EAAAhmed@imamu.edu.sa; dr.ehabsaleh@yahoo.com

<sup>1</sup> Department of Chemistry, College of Science, Imam Mohammad Ibn Saud Islamic University (IMSIU), Riyadh 11623, Saudi Arabia

<sup>2</sup> Chemistry Department, Faculty of Science, Benha University, Benha 13518, Egypt

<sup>3</sup> Department of Chemistry, College of Science, Princess Nourah bint Abdulrahman University, P.O. Box 84428, Riyadh 11671, Saudi Arabia

<sup>4</sup> Department of Chemistry, College of Sciences & Arts, King Abdulaziz University, Rabigh, Saudi Arabia

<sup>5</sup> Department of Chemistry, Faculty of Applied Sciences, Umm Al-Qura University, Makkah 21955, Saudi Arabia

<sup>6</sup> Microbiology and Immunology Department, Faculty of Pharmacy, Galala University, Galala City 11566, Suez, Egypt

<sup>7</sup> Microbiology and Immunology Department, Faculty of Pharmacy, Ahran Canadian University (ACU), Giza 12451, Egypt

<sup>8</sup> Department of Chemistry, College of Science, University of Jeddah, Jeddah 21589, Saudi Arabia

<sup>9</sup> Institute of Chemical Sciences, Gomal University, Dera Ismail Khan 29111, KPK, Pakistan

small concentrations [2–4]. Lead is utilized in a variety of industries, and large quantities of wastewater that contain high levels of Pb(II) ions are released in certain locations. Industries including electroplating, metallurgy, storage batteries, electronics, petroleum refining, and paint contribute significantly to pollution by releasing waste containing Pb(II) ions [5]. The allowable concentrations of Pb(II) ions in wastewater and drinking water have been established by the United States Environmental Protection Agency at 0.015 mg/L [6]. The allowable concentrations of Pb(II) ions in wastewater and drinking water have been established by the World Health Organization (WHO) at 10 µg/L [6]. Lead gets into ground and surface water either directly or indirectly, and it builds up in communities of living things. Lead accumulates primarily in muscles, kidneys, brain tissues, and bones, and can result in anemia, kidney diseases, and nervous system disorders [7–9]. To ensure a higher quality of life, it is important to eliminate Pb(II) ions from industrial effluents in order to reduce their concentration to an acceptable limit. Metal ions are removed from water utilizing filtration, ion exchange, adsorption, reverse osmosis, and chemical precipitation methods [10–16]. Among these techniques, adsorption is the most effective and cost-effective [17–19]. Several studies on the removal of Pb(II) ions from aqueous solutions using various adsorbents have been published. Zhu et al. synthesized xanthate-modified magnetic chitosan with a greatest uptake capacity of 76.90 mg/g for the removal of Pb(II) ions from water-based solutions [20]. In their study, Chen et al. prepared a composite material by crosslinking chitosan with epichlorohydrin. The composite exhibited a maximum uptake capacity of 34.13 mg/g for the disposal of Pb(II) ions from water-based solutions [21]. Joseph et al. synthesized FAU zeolite with a greatest uptake capacity of 109.89 mg/g for the removal of Pb(II) ions from water-based solutions [22]. In their research, Roy et al. fabricated maghemite nanotubes that displayed a maximum disposal capacity of 71.420 mg/g for removing Pb(II) ions from water-based solutions [23]. In recent times, various nanomaterials, including sodium magnesium silicate hydrate and sodium magnesium silicate hydroxide, have been employed for the elimination of both organic and inorganic pollutants [24, 25]. In terms of the crystal lattice structure of sodium magnesium silicate hydrate and sodium magnesium silicate hydroxide, the presence of divalent Mg(II) ions substitutes certain tetravalent Si(IV) ions, resulting in the generation of a negative charge that is balanced by the presence of positive sodium ions. Afterward, the positive Na(I) ions can then be easily replaced with further positive ions, such as methylene blue dye [24]. Therefore, in this paper, the hydrothermal technique is used for the facile fabrication of sodium manganese silicate hydroxide hydrate/manganese silicate nanocomposite ( $\text{Na}_4\text{Mn}_5\text{Si}_{10}\text{O}_{24}(\text{OH})_6 \cdot 6\text{H}_2\text{O}/\text{Mn}^{2+}\text{Mn}_6^{3+}\text{SiO}_{12}$ ) as a novel type of nanocomposites for the remarkable uptake

of Pb(II) ions from water-based solutions. The synthesized nanocomposite has a unique structure that makes it highly suitable for adsorbing Pb(II) ions from aqueous media. The synthesized nanocomposite possesses ion exchange properties due to the presence of exchangeable sodium cations within its structure. These exchangeable sodium cations can be replaced by Pb(II) ions, resulting in the immobilization of Pb(II) ions within the composite framework. Also, the internal network of channels and pores of the synthesized nanocomposite allows for the easy diffusion of Pb(II) ions into its structure. In terms of the crystal lattice structure of the synthesized nanocomposite, the presence of divalent Mn(II) ions substitutes certain tetravalent Si(IV) ions, resulting in the generation of a negative charge that is balanced by the presence of positive sodium ions. Afterward, the positive sodium ions can then be easily replaced with further positive ions, such as Pb(II) ions. Our research group aims to construct novel and effective adsorbents using a low-cost approach for removing large amounts of lead ions from water-based solutions. Compared to the aforementioned adsorbents used to remove Pb(II) ions in the literature, the chemicals used in synthesizing our new nanocomposite, such as sodium metasilicate pentahydrate, manganese acetate tetrahydrate, and polyethylene glycol 400, are inexpensive. In addition, no complicated equipment or difficult chemical processes are used. Additionally, adsorption effects such as contact time, pH, temperature, and concentration are also examined to optimize the environmental influences controlling the adsorption process.

## 2 Experimental

### 2.1 Chemicals

Sodium hydroxide (NaOH), lead nitrate ( $\text{Pb}(\text{NO}_3)_2$ ), manganese acetate tetrahydrate ( $\text{Mn}(\text{CH}_3\text{COO})_2 \cdot 4\text{H}_2\text{O}$ ), hydrochloric acid (HCl), sodium metasilicate pentahydrate ( $\text{Na}_2\text{SiO}_3 \cdot 5\text{H}_2\text{O}$ ), ethylenediaminetetraacetic acid disodium salt dihydrate ( $\text{C}_{10}\text{H}_{14}\text{N}_2\text{Na}_2\text{O}_8 \cdot 2\text{H}_2\text{O}$ ), and polyethylene glycol 400 ( $\text{H}(\text{OCH}_2\text{CH}_2)_n\text{OH}$ ) were gotten from Sigma Aldrich Chemical Company. These chemicals were consumed as purchased without any purifying method.

### 2.2 Fabrication of the Mn/Si Nanocomposites

A fresh solution of Si(IV) ions was made by dissolving 12.75 g of  $\text{Na}_2\text{SiO}_3 \cdot 5\text{H}_2\text{O}$  in about 80 mL of deionized water. To prepare a fresh solution of Mn(II) ions, 3.76 g of  $\text{Mn}(\text{CH}_3\text{COO})_2 \cdot 4\text{H}_2\text{O}$  was dissolved in 80 mL of deionized water. Afterwards, the solution of Mn(II) ions was added drop by drop to the solution of Si(IV) ions with strong stirring for about 20 min. Furthermore, polyethylene glycol 400

(8.5 mL) was gradually added drop by drop to the previous mixture with vigorous stirring for a duration of 20 min. In addition, the resultant gel was transferred into a Teflon-lined stainless-steel autoclave (Capacity = 180 mL) and hydrothermally treated at 180 °C for 12 h. The resultant nanocomposites were filtered, carefully washed several times with hot deionized water, dried in an oven at 60 °C, calcinated at 600 °C for 6 h, and coded as NP. The previous practical steps are repeated, but in the absence of polyethylene glycol 400, and the resulting sample is coded as NF.

### 2.3 Characterization

The X-ray diffraction (XRD) patterns of the NF and NP nanocomposites were acquired using a D8 Advance X-ray diffractometer equipped with a copper anode ( $\text{CuK}_\alpha$  wavelength of 0.15 nm). The Fourier transform infrared spectroscopy (FT-IR) spectra of the NF and NP nanocomposites were recorded using a Nicolet iS50 spectrophotometer over the range of 4000–400  $\text{cm}^{-1}$ . A JSM-IT800 Schottky field emission scanning electron microscope (FE-SEM) coupled with an energy-dispersive X-ray spectroscopy unit (EDX) was utilized to characterize the composition and morphology of the NF and NP nanocomposites. A Quantachrome nitrogen gas sorption analyzer of model Touch LX2/NOVA was carefully employed to determine the Brunauer, Emmett, and Teller (BET) surface area, total pore volume, and mean pore radius of the NF and NP nanocomposites. A Perkin Elmer atomic absorption spectrometer of model 3300 multi-element was utilized to measure the concentration of Pb(II) ions.

### 2.4 Elimination of Lead Ions from Aqueous Media

The adsorption processes of lead ions on the NP and NF adsorbents were evaluated using the batch adsorption technique. In this regard, a 100 mL solution of 150 mg/L Pb(II) ions was taken in a 250 mL conical flask then the primary pH was adapted using NaOH/HCl solutions. 0.05 g of the NP or NF adsorbents was added then the conical flask was shaken for the desired time using a DKS1020 shaking incubator. The NP or NF adsorbents were then separated by centrifugation, and the concentration of Pb(II) ions in the filtrate was measured. Several variables affecting the adsorption of Pb(II) ions on the NP and NF adsorbents, including pH (2.5–7), time (10–140 min), uptake temperature (25–55 °C), and primary concentration (100–250 mg/L), were investigated. Using a Perkin Elmer atomic absorption spectrometer of model 3300 multi-element, the initial and final concentrations of Pb(II) ions were measured at a wavelength of 283.31 nm.

The uptake percentage (% R) of Pb(II) ions and the uptake capacity (Q) of the NP and NF adsorbents were determined using Eqs. 1 and 2, respectively [26, 27].

$$\%R = \frac{C_o - C_{eq}}{C_o} \times 100 \quad (1)$$

$$Q = (C_o - C_{eq}) \times \frac{V}{W} \quad (2)$$

The symbols  $C_o$ ,  $C_{eq}$ , and  $W$  represent the initial concentration of Pb(II) ions (mg/L), the equilibrium concentration of Pb(II) ions (mg/L), and the dry mass of the NP or NF adsorbents (g), respectively. Also,  $V$  is considered the volume of the lead solution (L).

To determine the point of zero charge ( $\text{pH}_{\text{PZC}}$ ) of the NP and NF adsorbents, Khalifa et al. [19] conducted the following procedure: 0.15 g of either the NP or NF adsorbents were individually added to about 0.05 L of 0.025 M  $\text{KNO}_3$  solutions. In the pH range of 2 to 12, the initial pH ( $\text{pH}_i$ ) of the  $\text{KNO}_3$  solutions was systematically assessed. Following this, each mixture of adsorbent and  $\text{KNO}_3$  underwent magnetic stirring for a duration of 6 h. The determined final pH values ( $\text{pH}_f$ ) were then measured and plotted against the determined initial pH values ( $\text{pH}_i$ ). The pH at which a clear plateau was observed corresponds to the point of zero charge ( $\text{pH}_{\text{PZC}}$ ).

## 3 Results and Discussion

### 3.1 Identification of the Fabricated Nanocomposites

The X-ray diffraction patterns of the NF and NP nanocomposites were illustrated in Fig. 1A, B, respectively. In addition, the NP and NF nanocomposites consisted of sodium manganese silicate hydroxide hydrate (Chemical formula:  $\text{Na}_4\text{Mn}_5\text{Si}_{10}\text{O}_{24}(\text{OH})_6 \cdot 6\text{H}_2\text{O}$  and JCPDS No. 00-039-0405) and manganese silicate (Chemical formula:  $\text{Mn}^{2+}\text{Mn}_6^{3+}\text{SiO}_{12}$  and JCPDS No. 00-041-1367). The appearance of broad XRD peaks in the NF nanocomposite at  $2\theta = 50.39^\circ$ ,  $56.93^\circ$ , and  $67.39^\circ$  was due to the (336), (408), and (624) miller plane indices of the manganese silicate, respectively. Besides, the appearance of a broad XRD peak in the NF nanocomposite at  $2\theta = 33.25^\circ$  was due to the (143) miller plane indices of the sodium manganese silicate hydroxide hydrate. The XRD peaks in the NP nanocomposite at  $2\theta = 21.83^\circ$ ,  $25.61^\circ$ ,  $28.32^\circ$ ,  $33.20^\circ$ ,  $42.29^\circ$ , and  $52.76^\circ$  were due to the (033), (130), (040), (143), (4 0 13), and (5 1 14) miller plane indices of the sodium manganese silicate hydroxide hydrate, respectively. In addition, the XRD peaks in

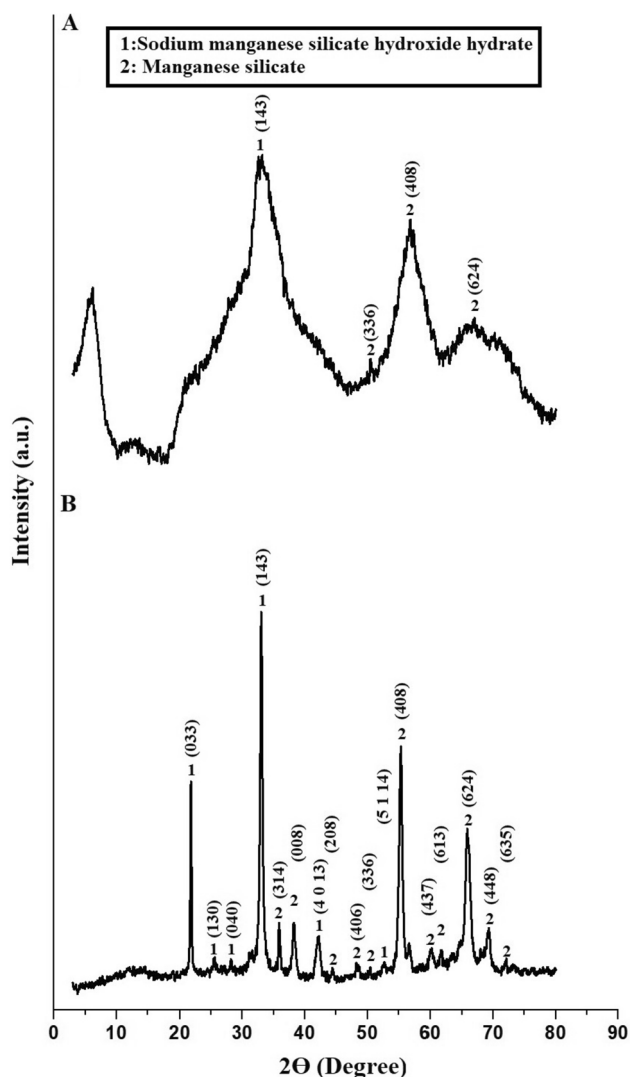


**Fig. 1** The obtained XRD patterns of the NF (A) and NP (B) nanocomposites

the NP nanocomposite at  $2\theta = 35.89^\circ, 38.35^\circ, 44.39^\circ, 48.39^\circ, 50.39^\circ, 55.49^\circ, 60.08^\circ, 61.62^\circ, 65.99^\circ, 69.17^\circ,$  and  $71.77^\circ$  were due to the (314), (008), (208), (406), (336), (408), (437), (613), (624), (448), and (635) miller plane indices of the manganese silicate, respectively. The mean crystallite sizes of the NF and NP nanocomposites were 18.28 and 60.26 nm, respectively. The NP sample has a more crystalline structure compared to the NF sample due to the effect of the organic template (i.e., polyethylene glycol 400). Organic templates, also known as structure-directing agents, are molecules that can interact with the growing crystal lattice during synthesis. They can influence the nucleation and growth processes of the crystals. In the presence of an organic template, the template molecules can guide the arrangement of atoms or molecules in a more organized manner, leading to better-defined crystal

structures. This results in improved crystallinity compared to samples without such guidance.

Figure 2A, B displays the FE-SEM images of the NF and NP nanocomposites, respectively. In the NF nanocomposite, spherical shapes with an average diameter of 15.32 nm can be observed, while the NP nanocomposite exhibits semi-spherical shapes and rods with an average diameter of 57.45 nm.

The patterns of EDX for the NF and NP nanocomposites are shown in Fig. 3A, B, respectively. The NP and NF nanocomposites consisted of O, Na, Si, and Mn, as presented in Table 1.

Figure 4A, B illustrates the FT-IR spectra of the NF and NP nanocomposites, respectively. The apparent absorption bands in the NF and NP nanocomposites at 448 and

**Table 1** Investigation of the NF and NP nanocomposites using EDX analysis

Sample	% O	% Na	% Si	% Mn
NF	28.48	14.57	27.81	29.14
NP	26.17	15.37	28.75	29.71

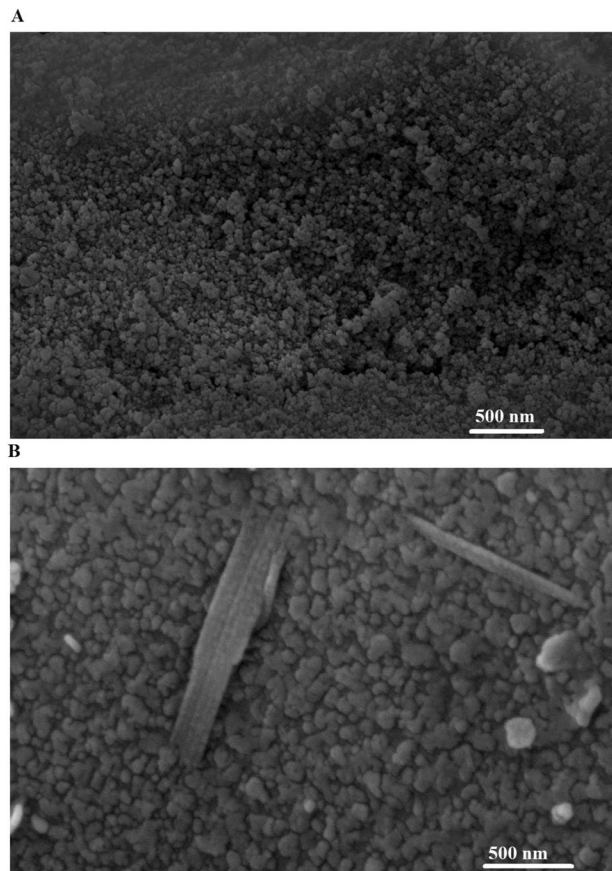


**Fig. 2** FE-SEM images of the NF (A) and NP (B) nanocomposites

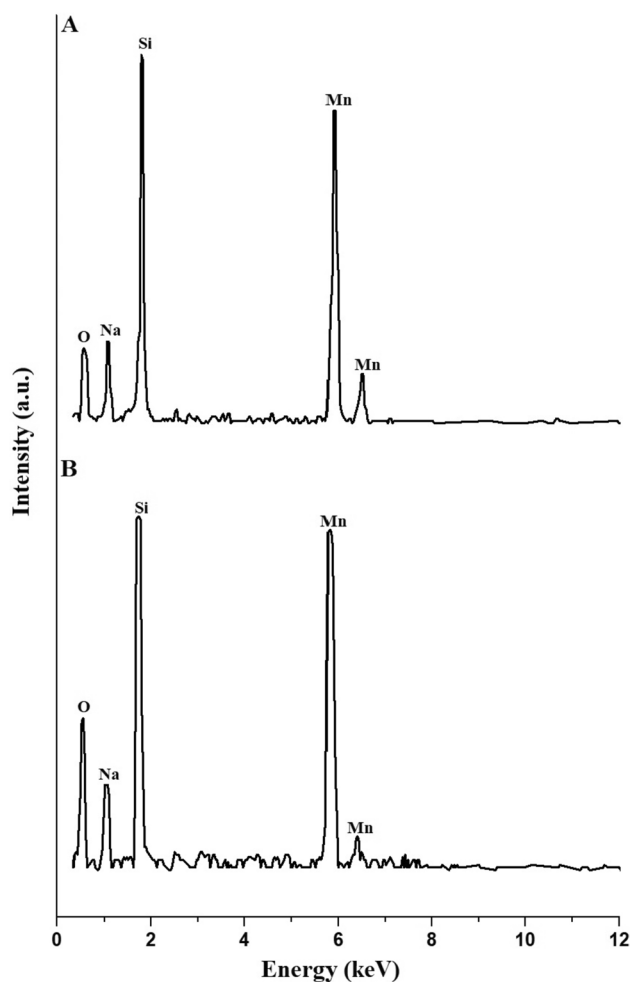


**Fig. 3** EDX patterns of the NF (A) and NP (B) nanocomposites

454  $\text{cm}^{-1}$  were associated to the bending vibration of the M–O–M (M = Mn and/or Si), respectively [24, 25, 28, 29]. The apparent absorption bands in the NF and NP nanocomposites at 619 and 614  $\text{cm}^{-1}$  were associated to the internal symmetric stretching vibration of the M–O–M (M = Mn and/or Si), respectively [24, 25, 28, 29]. The apparent absorption bands in the NF and NP nanocomposites at 789 and 780  $\text{cm}^{-1}$  were associated to the external symmetric stretching vibration of the M–O–M (M = Mn and/or Si), respectively [24, 25, 28, 29]. The apparent absorption bands in the NF and NP nanocomposites at 1024 and 1012  $\text{cm}^{-1}$  were associated to the internal asymmetric stretching vibration of the M–O–M (M = Mn and/or Si), respectively [24, 25, 28, 29]. The apparent absorption bands in the NF and NP nanocomposites at 1469 and 1413  $\text{cm}^{-1}$  were associated to the external asymmetric stretching vibration of the M–O–M (M = Mn and/or Si), respectively [24, 25, 28, 29]. The apparent absorption bands in the NF and NP nanocomposites at 1632 and 1644  $\text{cm}^{-1}$  were associated to the bending vibration of the OH, respectively [24, 25, 28–31]. The apparent

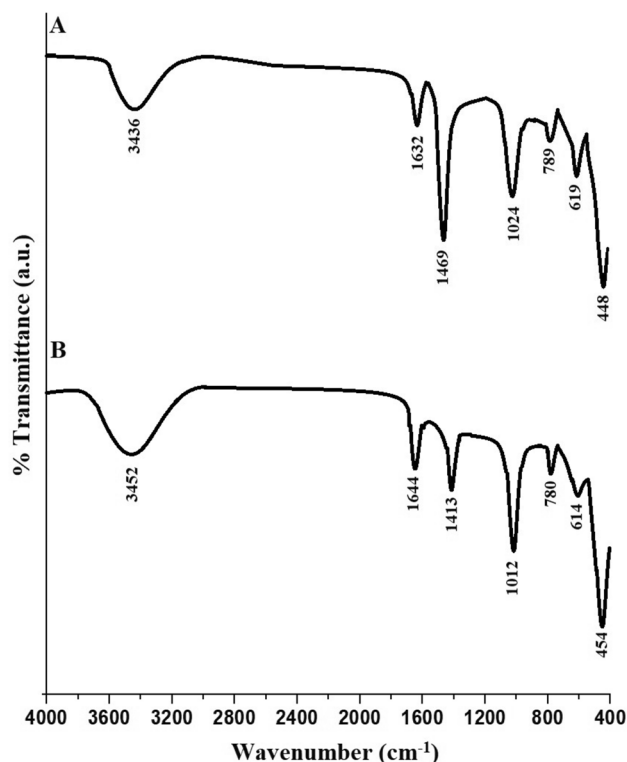


**Fig. 4** FT-IR spectra of the NF (A) and NP (B) nanocomposites

absorption bands in the NF and NP nanocomposites at 3436 and 3452  $\text{cm}^{-1}$  were associated to the stretching vibration of the OH, respectively [24, 25, 28–31].

Figure 5A, B represents the  $\text{N}_2$  adsorption/desorption of the NF and NP samples, respectively. In addition, the outcomes illustrated that the resultant curves of the NF and NP nanocomposites belong to the III types according to IUPAC adsorption patterns [13]. The textures of surface, such as average pore size, total pore volume, and BET surface area, were displayed in Table 2. In addition, the NF nanocomposite exhibited a higher BET surface area compared to the NP nanocomposite due to the inverse relationship between the determined crystallite size and the BET surface area. A substance with smaller crystallites is likely to have a larger number of grain boundaries, which can provide more surface area per unit mass. Therefore, when crystallite size decreases, the surface area tends to increase.

**Table 2** Textures of surface for the NF and NP nanocomposites

Sample	Average pore size (nm)	Total pore volume (cc/g)	BET surface area ( $\text{m}^2/\text{g}$ )
NF	2.81	0.1005	71.52
NP	3.09	0.0714	46.26

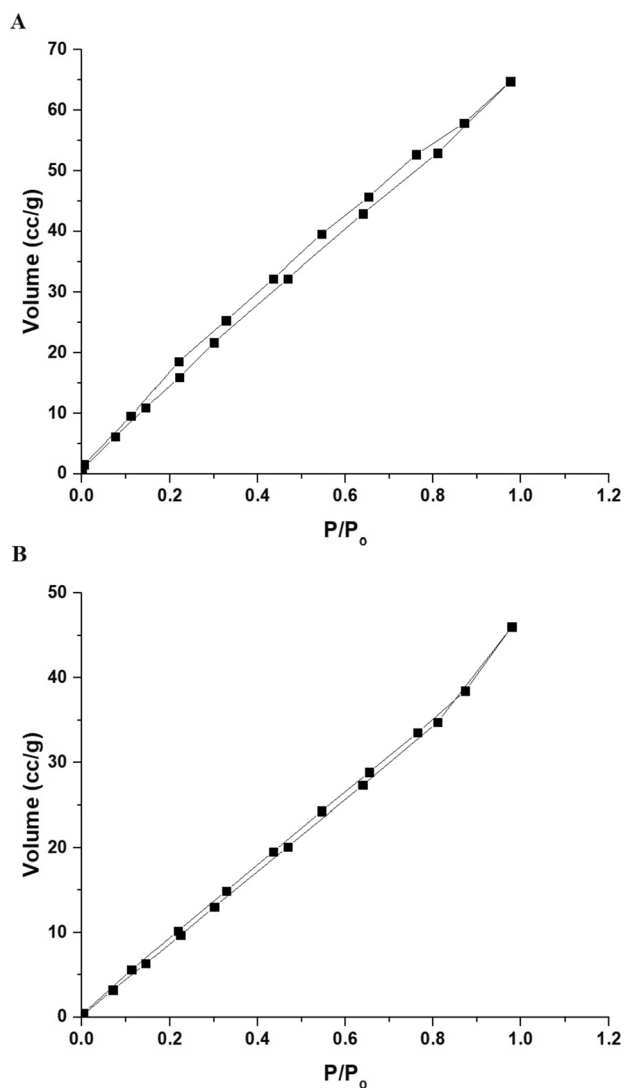


**Fig. 5** The obtained N<sub>2</sub> adsorption/desorption of the NF (A) and NP (B) nanocomposites

## 3.2 Elimination of Pb(II) Ions from Aqueous Media

### 3.2.1 Influence of Solution pH

The effect of solution pH on the uptake percentage of Pb(II) ions using the NF and NP nanocomposites was investigated by modulating the pH from 2.5 to 7 as shown in Fig. 6A. In addition, the point of zero charge ( $pH_{PZC}$ ) of the NF and NP nanocomposites is 6.24 and 6.53, respectively, as shown in Fig. 6B. The uptake percentage of Pb(II) ions increased with increasing solution pH and recorded its smallest and greatest values at pH 2.5 and 7, respectively. The uptake percentage of Pb(II) ions at pH 2.5 and 7 using the NF nanocomposite is 9.48 and 94.49%, respectively. The uptake percentage of Pb(II) ions at pH 2.5 and 7 using the NP nanocomposite is 3.29 and 67.75%, respectively. At pH values  $< pH_{PZC}$ , the

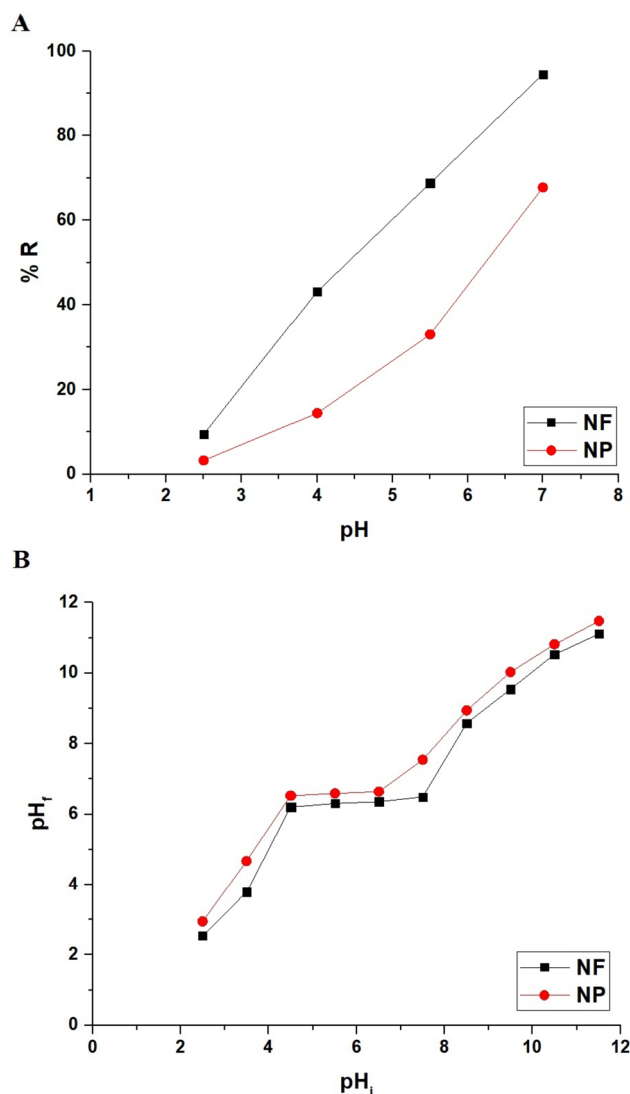


**Fig. 6** Effect of solution pH on the uptake percentage of Pb(II) ions using the NF and NP samples (A). The point of zero charge of the NF and NP samples (B)

positive hydrogen ions ( $H^+$ ) compete with the Pb(II) ions for adsorption sites on the NF and NP nanocomposites, resulting in the partial release of the Pb(II) ions and hence the uptake percentage of Pb(II) ions decreased. At pH values  $> pH_{PZC}$ , the concentration of positive hydrogen ions ( $H^+$ ) as competing ions decreases, leading to an increase in the uptake percentage of Pb(II) ions [12, 17]. The synthesized nanocomposites were not examined for the impact of pH levels above 7 on the elimination of Pb(II) ions, as these ions tend to precipitate beyond a pH of 7.

### 3.2.2 Influence of Contact Time

The effect of contact time on the uptake percentage of Pb(II) ions using the NF and NP nanocomposites was examined by

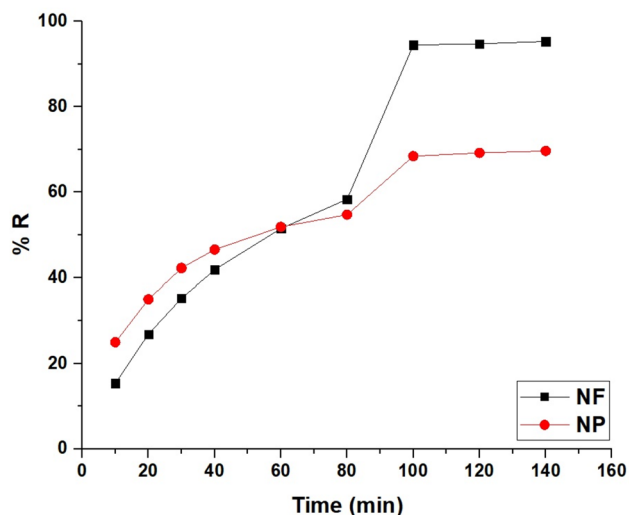


**Fig. 7** Impact of contact time on the uptake percentage of Pb(II) ions using the NF and NP nanocomposites

modulating the adsorption contact time from 10 to 140 min, as shown in Fig. 7. The uptake percentage of Pb(II) ions increased with increasing the contact time from 10 to 100 min because of the availability of the adsorption sites. As the adsorption contact time was extended from 100 to 140 min, the uptake percentage of Pb(II) ions stabilized due to the saturation of the uptake sites. In addition, the results revealed that the NF and NP nanocomposite exhibited rapid adsorption of Pb(II) ions as the adsorption contact time increased from about 80 to 100 min. However, the adsorption rate slowed down and reached a plateau as the adsorption time was further extended from 100 to 140 min. This behavior can be attributed to the strong electrostatic interaction between the nanocomposite surface and the Pb(II) ions, facilitating their quick dispersion and subsequent coverage of the adsorbent surface [32, 33].

To understand the uptake processes of lead ions by the NF and NP nanocomposites, the experimental data was evaluated by the pseudo-first-order (Eq. 3) and pseudo-second-order (Eq. 4) models [12, 17, 26, 27]. Figure 8A, B depicts the application of these models to the experimental data, respectively.

$$\log(Q_{eq} - Q_t) = \log Q_{eq} - \frac{k_F}{2.303} t \quad (3)$$

$$\frac{t}{Q_t} = \frac{1}{k_S Q_{eq}^2} + \frac{1}{Q_{eq}} t \quad (4)$$

In the context of the adsorption process,  $Q_t$  denotes the amount of Pb(II) ions adsorbed at time  $t$  (mg/g), while  $Q_{eq}$  represents the amount of Pb(II) ions adsorbed at equilibrium (mg/g). The pseudo-first-order rate constant is

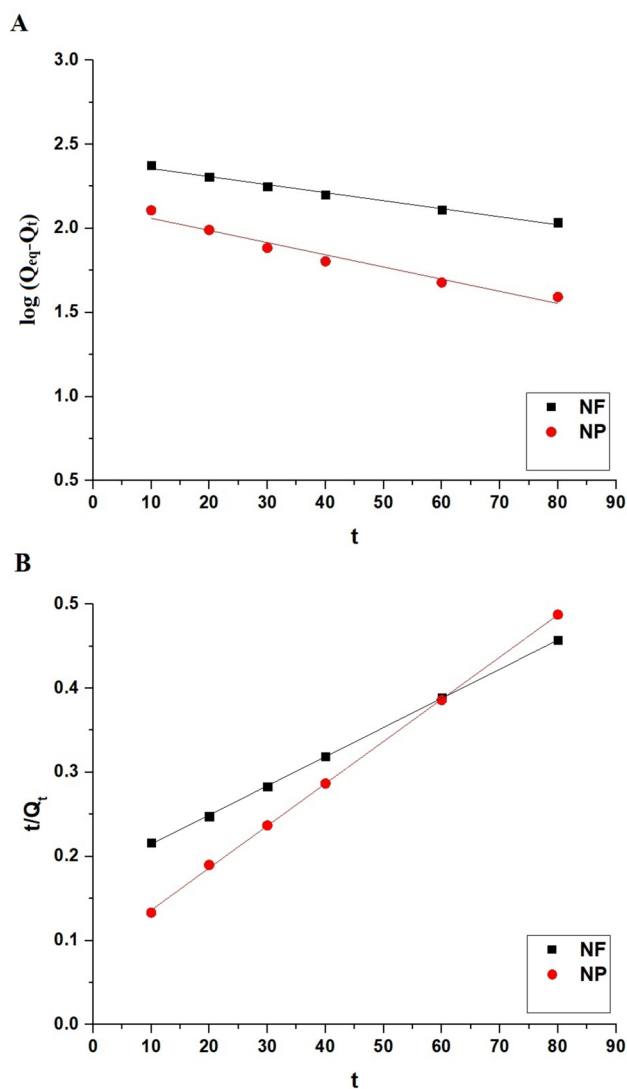


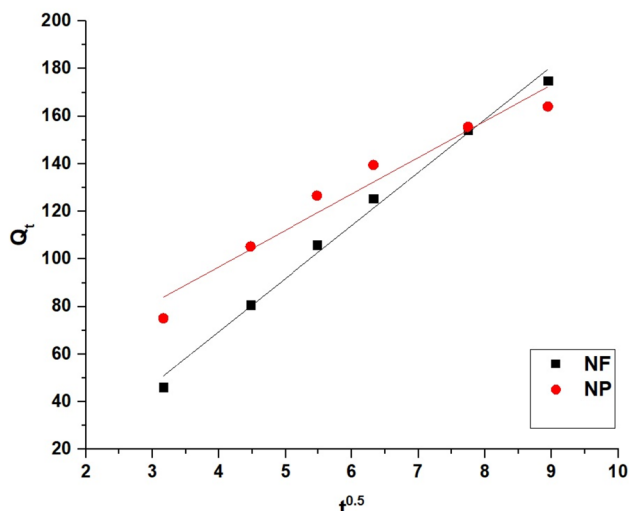
**Fig. 8** Representation of the kinetic outcomes utilizing the pseudo-first-order (A) and pseudo-second-order (B) models

represented by  $k_F$  (1/min), and the pseudo-second-order rate constant is denoted by  $k_S$  (g/mg.min). The kinetic constants were presented in Table 3. In comparison to the pseudo-second-order kinetic equation, the pseudo-first-order kinetic equation resulted in a weak fit with low correlation coefficient ( $R^2$ ) values, as clarified in Table 3. Furthermore, Table 3 clarified that the adsorption capacity values ( $Q_{eq}$ ) obtained through the pseudo-second-order model were significantly closer to the experimental values ( $Q_{exp}$ ) compared to those obtained through the pseudo-first-order model [34–36]. Therefore, the uptake of lead ions by the NF and NP samples may be best described by the pseudo-second-order model.

Furthermore, the diffusion mechanism was determined by applying the intraparticle diffusion model (Eq. 5) [13], as shown in Fig. 9.

**Table 3** Kinetic constants for the removal of Pb(II) ions using the NF and NP nanocomposites

Sample	Pseudo-first-order				Pseudo-second-order		
	$Q_{exp}$	$Q_{eq}$ (mg/g)	$k_F$ (1/min)	$R^2$	$Q_{eq}$ (mg/g)	$k_S$ (g/mg.min)	$R^2$
NF	283.46	253.45	0.0110	0.9854	288.18	6.69E-5	0.9998
NP	205.24	135.73	0.0167	0.9548	199.20	29E-5	0.9997

**Fig. 9** Illustrating the kinetic outcomes using the intra-particle diffusion kinetic model**Table 4** The constants related to the intraparticle diffusion kinetic model

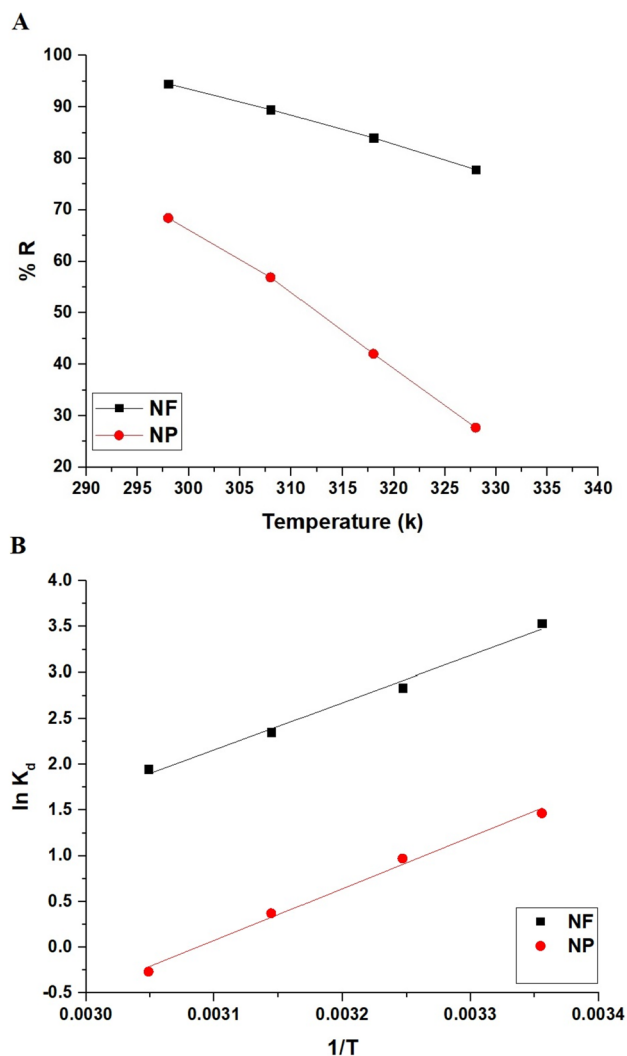
Sample	$k_1$ (mg/(g.min <sup>0.5</sup> ))	$C$ (mg/g)	$R^2$
NF	22.28	19.56	0.9916
NP	15.29	35.62	0.9418

$$Q_t = k_1 t^{0.5} + C \quad (5)$$

The internal diffusion constant, abbreviated as  $k_1$  (mg/(g.min<sup>0.5</sup>)), is the diffusion rate within the material, while the thickness of the boundary layer is exemplified by  $C$  (mg/g). Table 4 provides all the constants related to the intraparticle diffusion kinetic model. In addition, the results confirmed that the plot of  $Q_t$  versus  $t^{0.5}$  exhibited a linear association, but the lines did not cross the origin. In addition, this model supported evidence that intra-particle diffusion is not the primary mechanism managing the rate of the process [13].

### 3.2.3 Influence of Temperature

The influence of solution temperature on the disposal percentage of lead ions by the NF and NP nanocomposites was investigated by modulating the temperature from 298

**Fig. 10** Influence of solution temperature on the disposal percentage of lead ions utilizing the NF and NP nanocomposites (A). The Van't Hoff plot of  $\ln K_d$  versus  $1/T$  (B)

to 328 K, as shown in Fig. 10A. The uptake percentage of Pb(II) ions decreased with increasing temperature and recorded its smallest and greatest values at 328 and 298 kelvins, respectively. The uptake percentage of Pb(II) ions at 298 and 328 kelvins using the NF nanocomposite was 94.49 and 77.83%, respectively. The uptake percentage of Pb(II) ions at 298 and 328 kelvins using the NP nanocomposite was 68.41 and 27.70%, respectively. By employing Eqs. 6, 7, and



8, it is possible to calculate the thermodynamic constants, including the change in free energy ( $\Delta G^\circ$ , KJ/mol), change in enthalpy ( $\Delta H^\circ$ , KJ/mol), and change in entropy ( $\Delta S^\circ$ , KJ/mol.k), respectively [12, 17, 26, 27].

The slope and intercept of the Van't Hoff plot of  $\ln K_d$  versus  $1/T$  were used to calculate the values of  $\Delta H^\circ$  and  $\Delta S^\circ$  as shown in Fig. 10B.

Table 5 shows the calculated thermodynamic constants.

$$\ln K_d = \frac{\Delta S^\circ}{R} - \frac{\Delta H^\circ}{RT} \quad (6)$$

$$\Delta G^\circ = \Delta H^\circ - T\Delta S^\circ \quad (7)$$

$$K_d = \frac{Q_{eq}}{C_{eq}} \quad (8)$$

The distribution constant ( $K_d$ ) is expressed in units of L/g, while R represents the ideal gas constant (KJ/mol K). Furthermore, T denotes the temperature during the adsorption process, measured in kelvin. At all temperatures, the calculated  $\Delta G^\circ$  values for the uptake of Pb(II) ions onto the NF nanocomposite decreased from  $-77.23$  to  $-80.68$  kJ/mol. In addition, at all temperatures, the calculated  $\Delta G^\circ$  values for the uptake of Pb(II) ions onto the NP nanocomposite decreased from  $-90.71$  to  $-95.09$  kJ/mol. Negative Gibbs free energy for the uptake of lead ions by the NF and NP nanocomposites suggested the spontaneous nature of the uptake process. The negative value of  $\Delta H^\circ$  indicated that the uptake of Pb(II) ions using the NF and NP nanocomposites was exothermic. Usually,  $\Delta H^\circ > 40$  KJ/mol for chemical adsorption, whereas  $\Delta H^\circ < 40$  KJ/mol for physical adsorption. Hence, the uptake of lead ions by the NF and NP nanocomposites was chemical in nature. The positive value of  $\Delta S^\circ$  indicates an increased level of randomness at the solid/solution interface during the uptake of lead ions using the NF and NP nanocomposites. [12, 17].

### 3.2.4 Influence of Concentration

The influence of concentration on the disposal percentage of lead ions by the NF and NP nanocomposites was investigated by modulating the concentration of Pb(II) ions from 100 to 250 mg/L, as shown in Fig. 11. At lower initial concentrations, the uptake percentage of Pb(II) ions increased

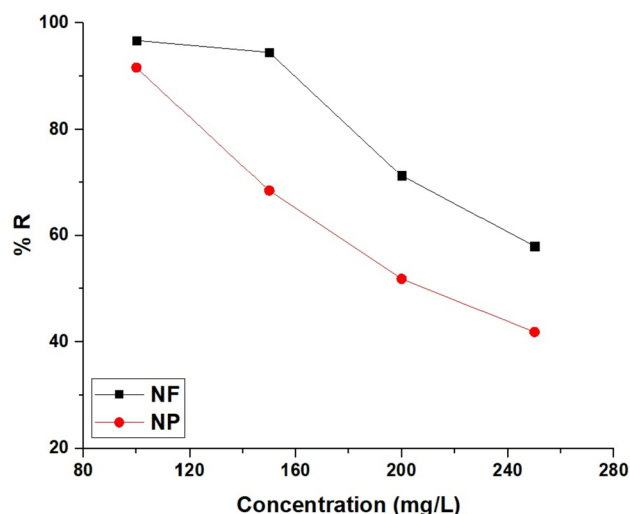


Fig. 11 Effect of initial concentration on the disposal percentage of lead ions by the NF and NP nanocomposites

as there were more active functional groups available. However, as the initial concentration increased, the adsorption sites eventually became saturated, leading to a decrease in the uptake percentage [34–36]. In order to understand the uptake processes of lead ions by the NF and NP nanocomposites, the experimental data was investigated by means of the Langmuir (Eq. 9) and Freundlich (Eq. 10) models [12, 17, 26, 27]. Figure 12A, B depicts the application of these isotherms to the experimental data, respectively.

$$\frac{C_{eq}}{Q_{eq}} = \frac{1}{k_1 Q_{max}} + \frac{C_{eq}}{Q_{max}} \quad (9)$$

$$\ln Q_{eq} = \ln k_2 + \frac{1}{n} \ln C_{eq} \quad (10)$$

The heterogeneity factor, denoted as n, quantifies the extent to which adsorption deviates from linearity. It represents the level of non-linearity between solution concentrations and adsorption. Adsorption is considered favorable when the value of n falls within the range of 1 to 10. The equilibrium constant of the Langmuir equation is denoted by  $k_1$  (L/mg). Additionally,  $k_2$  represents the equilibrium constant of the Freundlich equation (mg/g)(L/mg) $^{1/n}$ , where  $Q_{max}$  signifies the greatest uptake capacity of the Langmuir

**Table 5** Thermodynamic constants calculated for the removal of Pb(II) ions employing the NF and NP nanocomposites

Samples	R <sup>2</sup>	$\Delta H^\circ$ (KJ/mol)	$\Delta S^\circ$ (KJ/mol k)	$\Delta G^\circ$ (KJ/mol)			
				298	308	318	328
NF	0.9985	-42.94	0.1151	-77.23	-78.38	-79.53	-80.68
NP	0.9994	-47.25	0.1458	-90.71	-92.17	-93.63	-95.09

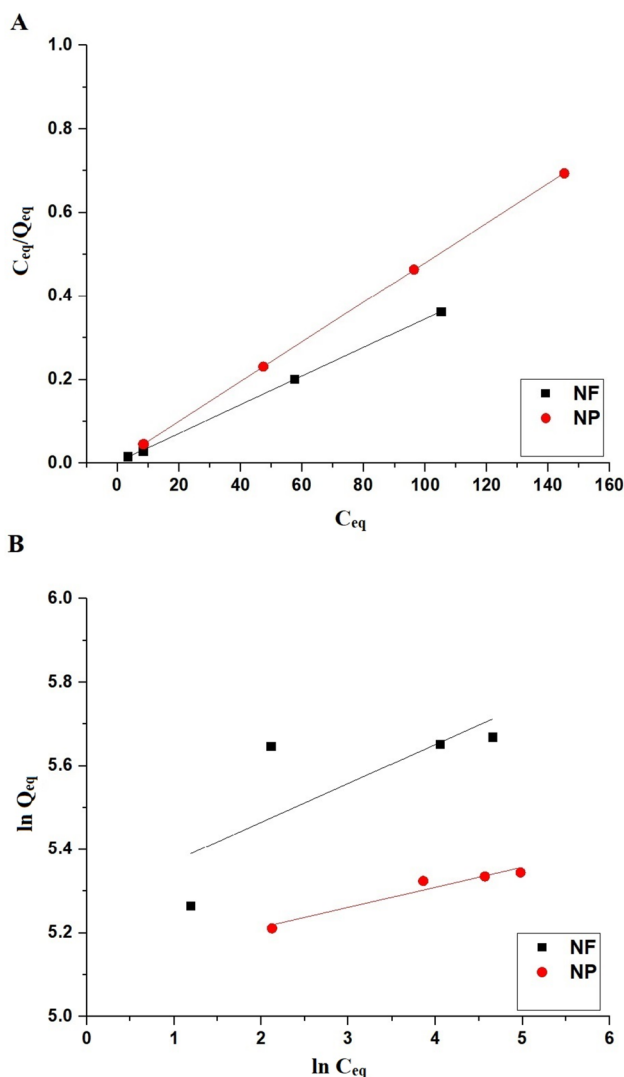


**Fig. 12** Presentation of the equilibrium outcomes using the Langmuir (A) and Freundlich (B) isotherms

equation (mg/g). Equation 11 can be employed to estimate  $Q_{max}$  from the Freundlich isotherm [12, 17, 26, 27].

$$Q_{max} = k_2(C_o^{1/n}) \quad (11)$$

Table 6 provides the equilibrium constants. In comparison to the Langmuir isotherm, the Freundlich isotherm resulted in a weak fit with low correlation coefficient ( $R^2$ )

**Table 6** Equilibrium constants determined for the adsorption of Pb(II) ions utilizing the NF and NP nanocomposites

Samples	Langmuir isotherm			Freundlich isotherm			
	$Q_{max}$ (mg/g)	$k_1$ (L/mg)	$R^2$	$Q_{max}$ (mg/g)	$k_2$ (mg/g)(L/mg) <sup>1/n</sup>	n	$R^2$
NF	292.39	0.9194	0.9997	312.79	196.23	10.74	0.3918
NP	210.97	0.7326	0.9998	212.21	166.87	20.88	0.9103

values. Therefore, the uptake of lead ions by the NF and NP nanocomposites may be best described by the Langmuir isotherm. Therefore, these findings suggest that the adsorption active sites were uniformly spread. The  $k_1$  value for the NF sample was higher than that of the NP sample, affirming the superior ability of the NF sample to eliminate lead ions.

The NF and NP samples exhibited maximum uptake capacities of 292.39 and 210.97 mg/g, respectively, for lead ions. Table 7 presents a comparative analysis of the adsorption capacity for removing lead ions using various adsorbents, including the newly fabricated nanocomposites [20–23]. The significant uptake capacity demonstrated by the NF and NP nanocomposites indicated their potential as promising adsorbents for efficient removal of lead ions.

### 3.2.5 Influence of Regeneration and Reusability

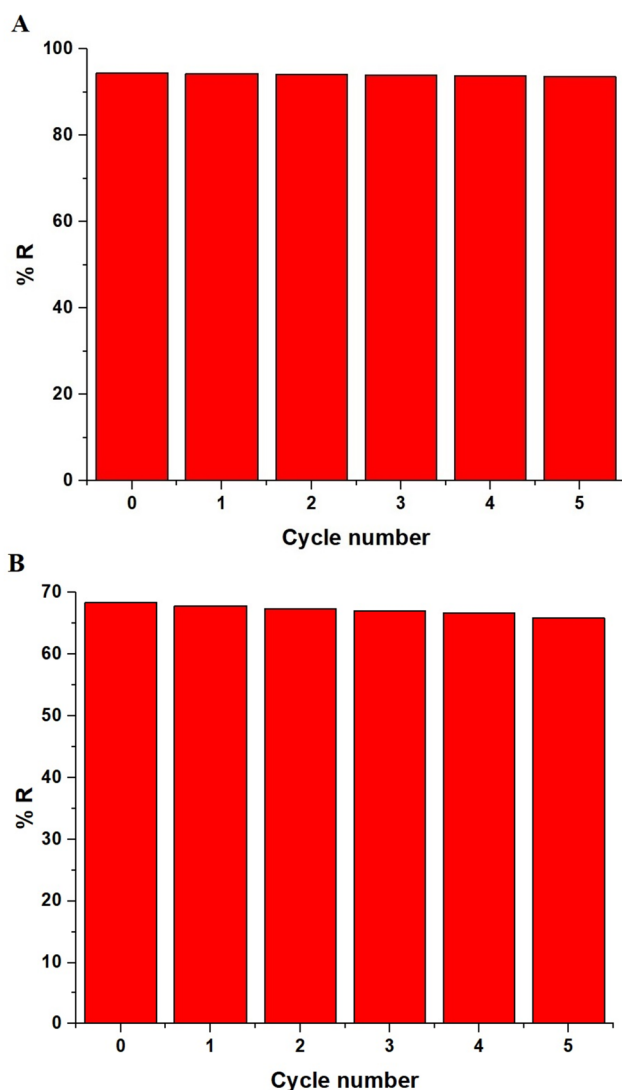
Considering the economic perspective, the regeneration and reusability of NF or NP adsorbents are critical factors. In this study, we successfully regenerated Pb(II)-loaded NF or NP by treating it with a 0.5 M solution of ethylenediaminetetraacetic acid disodium salt dihydrate, using a volume of 50 mL. Subsequently, the disposal method was meticulously carried out as previously described, and its effectiveness was evaluated. Figure 13A, B demonstrates the efficacy of NF and NP adsorbents during five consecutive adsorption/desorption cycles, respectively. Remarkably, even after undergoing five cycles, the adsorbent maintained its uptake percentage. Hence, due to their cost-effective synthesis, superior uptake capacity, and impressive regeneration efficiency, the NF and NP adsorbents emerge as practical choices for wastewater treatment.

### 3.2.6 Influence of Interfering Ions

The research focused on examining how other ions affect the effectiveness of the NF and NP adsorbents. To simulate real-world conditions, Na(I), K(I), Ca(II), and Mg(II) ions were chosen as representative interfering ions due to their presence in natural water and industrial wastewater. These interfering ions can compete with the target pollutants for adsorption sites, potentially reducing the adsorbents' efficiency. To assess this impact, varying concentrations of each interfering ion were individually mixed with a 150 mL solution containing 100 µg/L of Pb(II) ions. The disposal

**Table 7** Comparative study of different adsorption capacities for lead ions

Adsorbent	Uptake capacity (mg/g)	References
Xanthate-modified magnetic chitosan	76.90	[20]
Crosslinked chitosan/epichlorohydrin composite	34.13	[21]
FAU zeolite	109.89	[22]
Maghemite nanotubes	71.42	[23]
NF	292.39	This study
NP	210.97	This study

**Fig. 13** Reusability of the NF (A) and NP (B) nanocomposites for the uptake of lead ions

method, as described previously, was carefully executed and evaluated for its efficacy. The tolerance limit was established as the highest concentration of the interfering ion that led to a 5% extraction error. In addition, the data in Table 8 demonstrate that the adsorption performance of NF or NP nanocomposites towards Pb(II) ions is minimally affected by the investigated interfering ions. Consequently, the elimination method can be confidently employed for removing Pb(II) ions from actual samples containing multiple components.

### 3.2.7 Application of NF and NP Nanocomposites in Real Wastewater Treatment

The NF and NP adsorbents, as previously depicted in the experimental section, were employed under optimal experimental conditions to evaluate their usefulness in treating polluted water. In brief, approximately 0.05 g of either NF or NP samples were added carefully to around 100 mL of authentic wastewater obtained from the oxidation pond in the 10th of Ramadan City area, Egypt. In addition, the pH was regulated to 7, and the resultant mixture was then shaken for 100 min. In addition, the primary concentration of lead ions in the authentic polluted water was 0.75 mg/L. Besides, the results demonstrated that both the NF and NP adsorbents exhibited complete uptake of lead ions. Moreover, this outcome enhances the safety of polluted water for potential reuse and provides insights into the appropriate discharge of treated effluent into aquatic environments.

## 4 Conclusions

The sodium manganese silicate hydroxide hydrate/manganese silicate nanocomposite ( $\text{Na}_4\text{Mn}_5\text{Si}_{10}\text{O}_{24}(\text{OH})_6 \cdot 6\text{H}_2\text{O}/\text{Mn}^{2+}\text{Mn}_6^{3+}\text{SiO}_{12}$ ) was facilely synthesized using the hydrothermal method in the absence and presence of polyethylene glycol 400 as an organic template. The nanocomposite synthesized without polyethylene glycol 400 exhibited an average crystallite size and BET surface area of 18.28 nm and 71.52  $\text{m}^2/\text{g}$ , respectively. In addition, the nanocomposite synthesized with polyethylene glycol 400 showed an average crystallite size and BET surface area of 60.26 nm and 46.26  $\text{m}^2/\text{g}$ , respectively. Besides, the nanocomposite synthesized

**Table 8** Tolerance limit of several interfering ions that influence the uptake of Pb(II) ions

Interfering ion	Tolerance limit ( $\mu\text{g}/\text{L}$ )	
	NF	NP
Na(I)	2500	2600
K(I)	2800	2500
Ca(II)	2000	2200
Mg(II)	2400	2200

without polyethylene glycol 400 exhibited a maximum disposal capacity of 292.39 mg/g for Pb(II) ions, while that synthesized with polyethylene glycol 400 showed a greatest uptake capacity of 210.97 mg/g. In addition, the uptake percentage of Pb(II) ions increased with increasing solution pH from 2.5 to 7. In addition, the uptake percentage of Pb(II) ions increased with increasing contact time from 10 to 100 min because of the availability of the adsorption sites. The stability of Pb(II) ion uptake percentage remains constant as the adsorption contact time is extended from 100 to 140 min, indicating the saturation of adsorption sites. The uptake processes of lead ions using the synthesized nanocomposites were found to be chemical, exothermic, and best expressed by the pseudo-second-order kinetic model and Langmuir equilibrium isotherm. Remarkably, even after undergoing five cycles, the synthesized nanocomposites maintained its uptake percentage. Consequently, due to their cost-effective synthesis, superior uptake capacity, and impressive regeneration efficiency, the synthesized nanocomposites emerge as practical choices for wastewater treatment.

**Acknowledgements** Princess Nourah bint Abdulrahman University Researchers Supporting Project number (PNURSP2023R185), Princess Nourah bint Abdulrahman University, Riyadh, Saudi Arabia.

**Author Contributions** FKA (Preparing figures and tables-Writing the introduction-Experimental Work), HSA (Research review-Research writing-Experimental work), STA (Experimental work), FAS (Preparing tables and figures), RMA (Revision-Writing the introduction), GSE (Resources-Experimental work), KR (Revision), EAA (Experimental work-Idea-Research review-Research Writing). All authors reviewed the manuscript.

**Funding** Princess Nourah bint Abdulrahman University Researchers Supporting Project number (PNURSP2023R185), Princess Nourah bint Abdulrahman University, Riyadh, Saudi Arabia.

**Data Availability** All data generated or analyzed during this work are included in this published article.

## Declarations

**Competing Interests** The authors declare no competing interests.

**Ethical Approval** Not applicable.

**Consent to Participate** Not applicable.

**Consent for Publication** Not applicable.

## References

- H. Nagy, M. Fawzy, E. Hafez, A.E.D. Mahmoud, *Environ. Sci. Pollut. Res.* **2023**, 1–17 (2023)
- G. Lin, B. Zeng, J. Li, Z. Wang, S. Wang, T. Hu, L. Zhang, *Chem. Eng. J.* **460**, 35 (2023)
- B. Xiao, J. Jia, W. Wang, B. Zhang, H. Ming, S. Ma, Y. Kang, M. Zhao, *J. Hazard. Mater. Adv.* **10**, 100254 (2023)
- H. Xiang, X. Min, C.J. Tang, M. Sillanpää, F. Zhao, *J. Water Process. Eng.* **49**, 103023 (2022)
- V.E. Johnson, Q. Liao, B.W. Jallowide, R. Anaman, C. Amanze, P. Huang, W. Cao, C. Ding, Y. Shi, *Colloids Surf. Physicochem. Eng. Asp.* **663**, 1–10 (2023)
- P.K. Pandey, S.K. Sharma, S.S. Sambhi, *J. Environ. Chem. Eng.* **3**, 2604 (2015)
- Q. Cui, L. Li, Y. Cao, B. Yang, L. Liu, X. Dong, Y. Cha, H. Ruan, S. Tang, Q. Wang, *Environ. Pollut.* **320**, 121036 (2023)
- Y. Xu, T. Peng, Q. Zhou, J. Zhu, G. Liao, F. Zou, X. Meng, *Comp. Biochem. Physiol. Part. C Toxicol. Pharmacol.* **266**, 109550 (2023)
- Z. Wang, H. Zhao, Y. Xu, J. Zhao, Z. Song, Y. Bi, Y. Li, X. Lan, C. Pan, N.S. Foulkes, S. Zhang, *Sci. Total Environ.* **804**, 150185 (2022)
- A.S. Al-Wasidi, A.M. Naglah, F.A. Saad, E.A. Abdelrahman, *Arab. J. Chem.* **15**, 104178 (2022)
- A.S. Al-Wasidi, H.S. AlSalem, A.F. Alshalawi, A.M. Naglah, A. Al-Anwar, E.A. Abdelrahman, *Arab. J. Chem.* **15**, 104113 (2022)
- A.S. Al-Wasidi, A.M. Naglah, F.A. Saad, E.A. Abdelrahman, *Arab. J. Chem.* **15**, 104010 (2022)
- E.A. Abdelrahman, Y.G. Abou El-Reash, H.M. Youssef, Y.H. Kotp, R.M. Hegazy, *J. Hazard. Mater.* **401**, 123813 (2021)
- M.S. Chauhan, A.K. Rahul, S. Shekhar, S. Kumar, *Mater. Today Proc.* **78**, 1–6 (2022)
- H. Wang, S. Chen, Y. Dong, J. Sun, J. Wang, Y. Nie, *J. Water Process. Eng.* **52**, 103540 (2023)
- R.S. Al-Absi, M. Khan, M.H. Abu-Dieyeh, R. Ben-Hamadou, M.S. Nasser, M.A. Al-Ghouti, *Chemosphere.* **311**, 137043 (2023)
- E.A. Abdelrahman, A. Alharbi, A. Subaihi, A.M. Hameed, M.A. Almutairi, F.K. Algethami, H.M. Youssef, *J. Mater. Res. Technol.* **9**, 7900 (2020)
- E.A. Abdelrahman, R.M. Hegazy, *Microchem. J.* **145**, 18 (2019)
- M.E. Khalifa, E.A. Abdelrahman, M.M. Hassanien, W.A. Ibrahim, *J. Inorg. Organomet. Polym. Mater.* **30**, 2182 (2020)
- Y. Zhu, J. Hu, J. Wang, *J. Hazard. Mater.* **221–222**, 155 (2012)
- A.H. Chen, S.C. Liu, C.Y. Chen, C.Y. Chen, *J. Hazard. Mater.* **154**, 184 (2008)
- I.V. Joseph, L. Tosheva, A.M. Doyle, *J. Environ. Chem. Eng.* **8**, 103895 (2020)
- A. Roy, J. Bhattacharya, *Chem. Eng. J.* **211–212**, 493 (2012)
- A.S. Al-Wasidi, M.T. Basha, R.M. Alghanmi, E.S. Al-Farraj, E.A. Abdelrahman, *Separations* **10**, 88 (2023)
- A.S. Al-Wasidi, M.T. Basha, R.M. Alghanmi, E.S. Al-Farraj, E.A. Abdelrahman, *J. Inorg. Organomet. Polym. Mater.* **33**, 1005 (2023)
- A.E.D. Mahmoud, M. Hosny, N. El-Maghrabi, M. Fawzy, *Sustain. Environ. Res.* **32**, 1–16 (2022)
- A.E.D. Mahmoud, *J. Environ. Manage.* **270**, 110911 (2020)
- E.A. Abdelrahman, *J. Mol. Liq.* **253**, 72 (2018)
- F.K. Algethami, A.S. Al, W. Eida, S. Al Farraj, H.A. Katouah, E.A. Abdelrahman, *Discov. Nano.* **18**(1), 70 (2023)
- E.A. Abdelrahman, E.S. Al-Farraj, *Nanomaterials* **12**, 3992 (2022)
- A.S. Al-Wasidi, F.A. Saad, A.M. Munshi, E.A. Abdelrahman, *RSC Adv.* **13**, 5656 (2023)
- M. Verma, A. Kumar, K.P. Singh, R. Kumar, V. Kumar, C.M. Srivastava, V. Rawat, G. Rao, S. Kumari, P. Sharma, H. Kim, *J. Mol. Liq.* **315**, 113769 (2020)
- M. Verma, A. Kumar, I. Lee, V. Kumar, J.H. Park, H. Kim, *Environ. Pollut.* **304**, 119130 (2022)
- M. Verma, I. Lee, S. Sharma, R. Kumar, V. Kumar, H. Kim, *ACS Omega* **6**, 34624 (2021)
- M. Verma, M. Mitran, H. Kim, D. Vaya, *J. Phys. Chem. Solids* **155**, 110125 (2021)

36. M. Verma, I. Tyagi, R. Chandra, V.K. Gupta, *J. Mol. Liq.* **225**, 936 (2017)

**Publisher's Note** Springer Nature remains neutral with regard to jurisdictional claims in published maps and institutional affiliations.

Springer Nature or its licensor (e.g. a society or other partner) holds exclusive rights to this article under a publishing agreement with the author(s) or other rightsholder(s); author self-archiving of the accepted manuscript version of this article is solely governed by the terms of such publishing agreement and applicable law.